Linear Approximation for Mapping Remaining Wall Thickness Using a Magnetic Flux Leakage Sensor

Buddhi Wijerathna, Raphael Falque, Sarath Kodagoda, and Gamini Dissanayake
University of Technology Sydney, Australia
Buddhi.Wijerathna@uts.edu.au

Abstract

Use of an unconventional sensor for mapping the remaining wall thickness of a pipe is presented in this paper. This is achieved through the development of a sensor model relating the measurements from a Magnetic Flux Leakage (MFL) sensor to the environment geometry. Conventional sensors, such as laser-range finders commonly used in the robotic community are not able to infer thickness profiles of ferromagnetic structures such as water pipes when the surface is covered with corrosion products. Sensors based on electromagnetic principles or ultrasound are the methods of choice in such situations to estimate the extent of corrosion and predict eventual failure. The general relationship between readings from electromagnetic sensors and the environment geometry is governed by a set of partial differential equations (Maxwells equations). However, in the case of an MFL sensor, it is demonstrated that a linear combination of the thickness profiles can be used to adequately model the sensor signal. Parameters associated with the sensor model are obtained using a two-dimensional finite element simulations. Extensive simulation results are presented to validate the proposed method by estimating a remaining wall thickness map of a realistic pipe.

1 Introduction

Non Destructive Evaluation (NDE) has been a focus of the researchers for a long time. The industrial need for reliable asset inspection techniques has grown with the complexity of the infrastructure and increased costs to maintain them. Difficulty in accessing the assets and related occupational health and safety issues have created an apparent demand for unmanned and remote condition assessment. With the advancement of robotic technologies, now it is evident to apply robotic solutions to the ever increasing condition assessment demand. Mission critical industries such as petrochemical and water supplies require reliable in-service inspection where the service cannot be terminated for regular inspection purposes. In-line robotic inspection tools have been used for this purposes of collecting crucial data while travelling inside the assets.

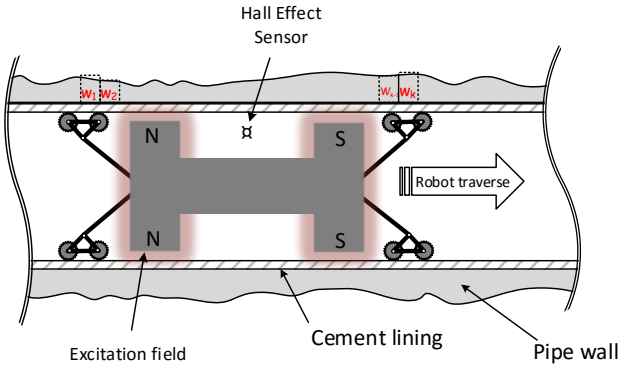

Figure 1: Representation of an in-line MFL inspection robot.

There is a wide range of NDE sensing techniques currently used in the industry for condition assessment of metallic infrastructure. To name a few, Remote Field Eddy Currents (RFEC), Pulsed Eddy Currents (PEC), Ultrasonic Technology (UT) and MFL are such technologies. MFL is widely used as in-line pigging robots due to its robustness and accuracy [Khodayari Rostamabad *et al.*, 2009]. In MFL technology, the ferromagnetic medium (*i.e.* the pipe wall) is magnetically saturated using a strong magnetic excitation. Both electro-magnets, as well as strong permanent magnets, are being used in practice for this purpose. Once the pipe walls are saturated, the flux lines are tightly packed within the structure while the magnetic field strength in the surrounding environment remain near zero. When there is a defect causing a reduction in the remaining wall thickness, there is leakage flux that can be measured using a

Hall effect or a Giant Magnetoresistance (GMR) sensor placed near the pipe surface. These sensor measurements can be used to estimate the thickness of the pipe wall. The MFL tool can be designed as an in-line tool or as an external scanning tool, however, this paper is focussed on its use as an in-line robotic inspection tool (Figure 1).

In the water industry, most of the ferromagnetic pipes are factory cement lined. These cement lines isolate the pipe walls from the water and contribute heavily to protect it from corrosion. Moreover, the internal cement lining provides an added advantage for the in-line robots to traverse smooth and to maintain constant sensor lift-off except for some exceptional cases where the cement lining is damaged or tuberculation present in the pipes. In these cases, pipes need to be pre-cleaned to use the in-line robots. The external walls are prone to heavy corrosion due to several factors including exposure to soil and moisture conditions over a long period of time. Therefore, it is reasonable to assume that the pipe wall losses are mainly due to external corrosion. In this work, we made an attempt to estimate the remaining wall thickness map of a pipe given the MFL signals measured using an in-line robotic inspection tool traversing along the pipe.

The remaining wall thickness of the pipe surfaces are related to the measured MFL signal. The critical difference when compared with traditional robotic sensors such as laser range finders or sonars is that while the sensor reading depends on the sensor location and environment geometry, the mapping from sensor space to Euclidean space is indirect, typically governed by the underlying physics expressed as a set of partial differential equations (Maxwell equations). Therefore information gathered from these sensors does not lend itself easily to reconstructing the environment geometry or localising the sensor or performing SLAM using existing techniques for robotic perception. Further, sensor lift-off, material properties and excitation intensity also affect the measurements. Hence inferring the remaining wall thickness map of the pipe from the signal information is a challenging task, unless the pipe geometry is relatively simple. This significant gap in the current knowledge is key to this paper.

Estimating the pipe wall profile from the MFL signal corresponds to solving the inverse problem. Many researches attempted to solve the inverse problem using analytical models [Minkov *et al.*, 2002; Mandache and Clapham, 2003] as well as machine learning methods. Artificial neural networks [Carvalho *et al.*, 2006] and Gaussian Processes [Wijerathna *et al.*, 2013] are reported few examples. Most of these approaches use data-driven techniques and do not recover the full thickness profile with few exceptions where iterative solvers are used [Wijerathna *et al.*, 2015]. However, current findings in water pipe condition assessment [Rathnayaka *et al.*, 2016] suggest that knowledge of patches or continuous thickness profiles are very useful in estimating the remaining life of the pipes. In this work, to enable simple hardware design, we assume a simple exciter arrangement along with the hall sensors in the middle of the exciters in a stationary scenario. The aim of this work is to formulate the forward and inverse MFL sensor model using a linear least-squares system and recover the entire remaining wall thickness profile of the pipe. As the data is associated with the odometry, the defects can be localised.

The rest of the paper unfolds as follows. Section 2 describes the behaviour of the MFL signal along with an analytical model from literature. The Finite Element Analysis (FEA) model is introduced next followed by the validations. The proposed linear least squares forward model and inverse sensor models are described next. Section 3 demonstrates the results evaluation of the forward and inverse models followed by a discussion of the performance and the limitations of the proposed method.

2 Sensor model for MFL

The forward problem of MFL phenomenon consists of mapping the cross-sectional pipe wall thickness to the Hall Effect sensor measurement through a sensor model. On the other hand, the inverse problem consists of finding the model that maps the sensor measurements to the cross-sectional remaining pipe wall thickness. The main goal is to solve the inverse problem, however solving the forward model gives a good insight into the behaviour of the sensory system. The forward model can be used as the basis to formulate the inverse model. Before presenting the proposed forward and inverse models, a basic analytical model will be presented to describe the MFL signal behaviour. A reasonably wide Region of Interest (ROI) has been selected to understand how the defect geometry affects sensor measurements near the surrounding area. Quantitative sophisticated models and analysis about the MFL signal behaviour are broadly discussed in literature [Uetake and Saito, ; Förster, 1986; Ireland and Torres, 2006], however, in this work axial component of the leakage flux alone is analysed.

2.1 Analytical Model

Following derivation assumes that a Dipolar Magnetic Charge (DMC) is developed on the defect faces intersecting the exciting magnetic field as a result of its interaction with the excitation field and follows the method as described in [Mandache and Clapham, 2003; Edwards and Palmer, 1986]. Additionally, it is assumed that the higher excitation intensity minimises the effects of variations in magnetisation and permeability of the material.

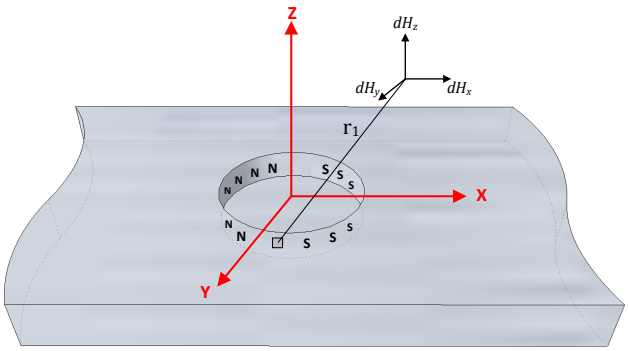

Figure 2: Dipolar magnetic charge model for a cylindrical defect.

A cylindrical defect with its axis aligned to Z direction has been considered as schematically represented in Figure 2. The magnetic flux flow around the defect creates a DMC on the side walls of the cylinder. The test substance is aligned to the xy plane with the top surface at $z = 0$. The depth of the flat bottom defect is represented by b_1. The MFL signal is measured above the test substance *i.e* $z > 0$.

$x < 0$ internal area of the cylindrical defect wall develops a positive magnetic charge density, $+\sigma$, while $x > 0$ area develops a negative magnetic charge density,$-\sigma$. The angle θ_1 is measured from the positive y direction. The differential element of charge at the defect, dp_1, has coordinates $(R_1 sin\theta_1, R_1 cos\theta_1, z_1)$ and a charge proportional to its area. The magnetic field (dH_1) generated at a distance r_1 by this element of charge dp_1 is given by

$$dH_1 = \frac{dp}{4\pi r_1^3}\mathbf{r_1}. \tag{1}$$

Now considering the positive polarity side H^+ of the defect and the axial component of the field at a distance r_{1+} are given by,

$$dH_x^+ = \frac{\sigma R_1 d\theta_1 dz_1}{4\pi r_1^3}\left(x + R_1 sin\theta_1\right), \tag{2}$$

where,

$$r_1 = \sqrt{\left(x + R_i sin\theta_1\right)^2 + \left(R_i cos\theta_1\right)^2 + \left(h - z_1\right)^2}. \tag{3}$$

Similarly, the negative polarity side leakage field H^- of the defect is given by,

$$dH_x^- = -\frac{\sigma R_1 d\theta_1 dz_1}{4\pi r_1^3}\left(x - R_1 sin\theta_1\right). \tag{4}$$

The y component of the leakage field, dH_y^+, vanishes due to the symmetry. The Equation 2 is integrated over θ_1 from 0 to π and over z from $-b1$ $(b > 0)$ to 0 to determine the total field at r_{1+} due to the positively polarised side of the defect, which leads to

$$H_z^+ = \int_0^{\pi}\int_{-b1}^{0} \frac{\sigma R_1 (h - z_1)}{4\pi\left\{\left(x + R_i sin\theta_1\right)^2 + \left(R_i cos\theta_1\right)^2 + \left(h - z_1\right)^2\right\}^{\frac{3}{2}}} dz_1 d\theta_1 \tag{5}$$

By using the same integration for the negatively polarised side $H_z^-$of the cylinder, the total normal leakage field along the x axis profile is given by,

$$dH_z = dH_z^+ + dH_z^- + dH_D(x, y, z). \tag{6}$$

In practical settings, there can be a non-zero MFL value appearing due to the direct coupling of the flux generated by the exciter coils to the sensor. Similar to the Equation (1), this field is also a function of the distance to the exciter poles. Therefore, a $dH_D(x, y, z)$ value is introduced to the equation to compensate for this effect.

2.2 Finite Element Analysis Model

This section describes the FEA model developed using the commonly used COMSOL Multiphysics software. Figure 3 shows the meshing of the FEA simulation model created using the AC/DC module of COMSOL Multiphysics software.

The FEA geometry is composed of four different components: (1) the air box defining the limits of the FEA scenario, (2) the exciter coil, which is modelled as an equivalent rectangular permanent magnet, (3) the Hall-effect sensor which is simplified to a point measurement (*e.g.* it could simulate a hall effect sensor), and (4) the pipe cross-sectional profile defined from pipe segments extracted from the decommissioned pipeline.

The air and steel pipe material properties are defined using built-in materials from the COMSOL library and assumed to be homogeneous and isotropic. The material properties used in the model are displayed in Table 1. The conductivity of the air is set to a non-zero value to avoid computational singularities.

Table 1: Properties of each material

material	μ_r	ϵ_r	ρ [S/m]
Air	1	1	10
Steel	B-H curve	1	1×10^7
Copper (coil)	1	1	5.99×10^7

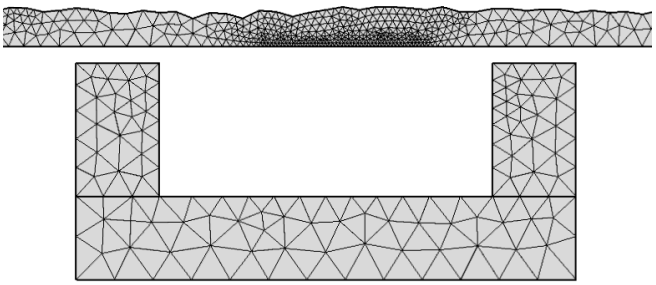

Figure 3: Free tetrahedral mesh in FEA simulation

In a practical setting, two coils are wound in a U-shaped yoke. These coils are used to excite the test substance by injecting magnetic flux. The measurements are taken as the tool moves along the pipe along the axial direction. Following the general practice, the computation time of the simulation set up was managed by replacing the coils with equivalent permanent magnets. Moreover, the 3D MFL tool was approximated with a 2D MFL model [Priewald *et al.*, 2013].

By defining a fixed sensor position and linear depth sampling, repeatability of the simulated measurements is achieved. A free-tetrahedral mesh, consisting of 2.5×10^4 elements is automatically generated by the simulation software (Figure 3). The solution is extracted when the "relative tolerance" of each consecutive iteration goes below 0.1%.

Similar to the practical scenario described in Section 1, the simulation model moves along the pipe collecting MFL signal data. The simulation model is iteratively used to generate the MFL signal as the tool travels along the pipe.

First, the FEA model was used to simulate the simple cylindrical defect scenario described in Section 2.1. Both analytical and FEA models were in agreement with the leakage flux distribution. This validates the FEA model and will be used for generating data for the formulations described in this work.

It is to be noted that the validated curve indicates a positive flux leakage magnitude in the close proximity to the defect. This implies that in a complex defect scenario, not only the spot thickness value underneath the sensor location but also the surrounding thickness profile affects a given spot measurement.

2.3 Forward Sensor Model

First we formulate the forward sensor model as a function of the thickness values in the close proximity of the travelling MFL tool. The following formulation follows

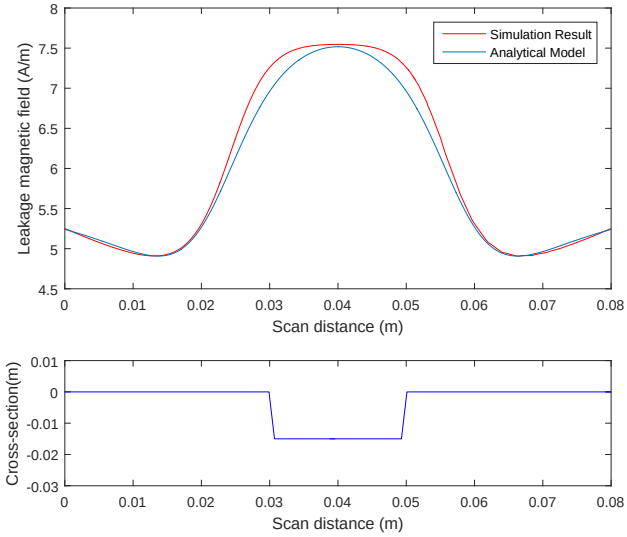

Figure 4: Comparison of Analytical model and Simulation

the framework proposed by [Falque *et al.*, 2016]. The ROI window of the ground truth profile moves as the tool travels along the pipe. The process consists of finding a function h such that $h : \boldsymbol{t} \longrightarrow y$, where y is the sensor measurements and $\boldsymbol{t}$ a set of thickness values that describe the pipe's cross-sectional geometry around the MFL tool.

Lets first consider a point measurement. According to the above observation, a point measurement is affected by the surrounding cross-sectional profile.

$$y = y_0 + \sum_{i=1}^{k} w_i t_i + \epsilon. \tag{7}$$

For a given sensor location with respect to the exciter coils, the direct coupling field contributes equally to all the measurements which are reflected by the y_0 constant term. t_i is the i^{th} thickness value of the piecewise constant thickness profile shown in Figure 1, and w_i is the unknown weight that relates to the location of the thicknesses for a given measurement. Furthermore, the noise ϵ relates to the sensor noise and the overlooked non-linearity. Given enough independent measurements, the optimal values for the weights can be found using a least square formulation.

Now consider a situation where m number of measurements were taken where each measurement is associated to k local discrete thickness that are regularly spaced over the ROI. This can also be interpreted as moving the tool inside the pipe simultaneously collecting MFL data in a moving window. The moving window approximates the thickness profile as a piecewise-constant profile as describe in Figure 1. We then formulate Equation (7)

in a matrix form to combine the m set of measurement and thickness values together,

$$\boldsymbol{y} = \boldsymbol{T}\boldsymbol{w} + \boldsymbol{\epsilon}, \tag{8}$$

where the constant term y_0, defined in Equation (7), could be calculated as it depends on the excitation intensity, number of turns in the coil, the electromagnetic properties of the material and the sensor location with respect to the exciter coils. It is, however, possible to estimate y_0 from the measurements themselves, therefore, we include it into the vector of the model parameters $\boldsymbol{w}$ which is defined as,

$$\boldsymbol{w} = \begin{bmatrix} y_0 \\ w_1 \\ \vdots \\ w_{k-1} \\ w_k \end{bmatrix}. \tag{9}$$

As discussed in Equation (7) , the piecewise thickness values of the each ROI are contained in $\boldsymbol{T}$

$$\boldsymbol{T} = \begin{bmatrix} 1 & t_{11} & t_{12} & \dots & t_{1k} \\ 1 & t_{21} & t_{22} & \dots & t_{2k} \\ \vdots & \vdots & \vdots & \ddots & \vdots \\ 1 & t_{m1} & t_{m2} & \dots & t_{mk} \end{bmatrix} \tag{10}$$

and the sensor point measurements associated with each ROI locations are contained in the $\boldsymbol{y}$ the vector

$$\boldsymbol{y} = \begin{bmatrix} y_1 \\ y_2 \\ \vdots \\ y_m \end{bmatrix}. \tag{11}$$

A wider ROI allows to select parameters $\hat{\boldsymbol{w}}$ that mostly reflects the magnetic field in a given ROI. As expected, it is observed that $\hat{\boldsymbol{w}}$ values near the sensor position have an higher impact and reaches to 0 as the distance from the Hall sensor increases. Therefore a reasonably high ROI should be selected for better results. So the optimisation can be summarised as

$$\min \left[\| \boldsymbol{T}\hat{\boldsymbol{w}} - \boldsymbol{y} \|^2 \right], \tag{12}$$

with $\hat{\boldsymbol{w}}$ the weight parameters, which are calculated to best fit $\boldsymbol{y}$ with least squares error. After calculating the weight parameters $\hat{\boldsymbol{w}}$ the forward solution can be evaluated by back calculating the estimated $\hat{y}$ as

$$\hat{\boldsymbol{y}} = \underbrace{\boldsymbol{T}\hat{\boldsymbol{w}}}_{h(\boldsymbol{T})}, \tag{13}$$

with the proposed model $h(\boldsymbol{T})$.

2.4 Inverse Sensor Model

Given the parameters of the forward model (7), we now consider the inverse problem. The goal is to find the inverse function h^{-1} such that $h^{-1} : \boldsymbol{y} \longrightarrow \boldsymbol{t}$. The following derivation flows the formulation proposed by [Falque *et al.*, 2016]. As described in Section 2.2 a wide window of thickness values in the ROI are contributing to the measurement. Hence h cannot be simply inverted. Instead, having the forward problem expressed as a linear model, allows formulating the inverse problem as a pseudo-inverse closed-form solution.

The goal of this section is to solve the inverse sensor model to come up with a cross-sectional thickness map for the full scan length. To solve the inverse problem, there should be more equations than the number of unknown parameters.

In a typical inspection setting, the MFL tool travels along the pipe collecting data associated with odometry. Let's assume during the inspection, a set of m discrete measurements were collected at regular intervals along the pipe. The pipeline geometry is approximated as a piecewise-constant profile with n steps of average thickness t.

Equation (7) can then be re-formulated as a global optimisation problem, where all the sensor measurements $\boldsymbol{y}$ are related to all the piecewise thicknesses t_i as

$$\boldsymbol{y} = \boldsymbol{W}\hat{\boldsymbol{t}} + \boldsymbol{y_0}, \tag{14}$$

$\hat{\boldsymbol{t}}$ represents the thickness estimation of the entire piecewise-constant pipeline profile,

$$\hat{\boldsymbol{t}} = \begin{bmatrix} t_1 \\ t_2 \\ \vdots \\ t_n \end{bmatrix}. \tag{15}$$

Thickness values and the sensor measurements are correlated by the $m \times n$ matrix $\boldsymbol{W}$, which is formulated with the parameters of the forward model. For each measurements, the corresponding line $\boldsymbol{W}$ is defined by the weights $\boldsymbol{w}$ for the defined ROI and set to 0 for the rest of the line. Since there are multiple measurements between the i^{th} and $(i+1)^{th}$ values, spatial weights $\overline{a_i}$ and $\overline{b_i}$ are used to derive the effective piecewise thickness profile for each measurement.

$$\boldsymbol{W} = \begin{pmatrix} \begin{pmatrix} & & \\ & U & \\ & & \end{pmatrix} & \begin{matrix} 0 \\ \vdots \\ 0 \end{matrix} & & \\ \begin{matrix} 0 \\ \vdots \\ 0 \end{matrix} & \begin{pmatrix} & & \\ & U & \\ & & \end{pmatrix} & & \\ & & \ddots & \\ & & & \begin{matrix} 0 \\ \vdots \\ 0 \end{matrix} \begin{pmatrix} & & \\ & U & \\ & & \end{pmatrix} \end{pmatrix}, \tag{16}$$

with U defined as:

$$\boldsymbol{U} = \begin{bmatrix} \overline{a_1} w_1 & \overline{b_1} w_1 + \bar{a_1} w_2 & \dots & \overline{b_1} w_k \\ \vdots & \vdots & & \vdots \\ \overline{a_j} w_1 & \overline{b_j} w_1 + \overline{a_j} w_2 & \dots & \overline{b_j} w_k \end{bmatrix}, \tag{17}$$

and $\bar{a_i}$ and $\bar{b_i}$ defined as

$$\bar{a_i} \triangleq \frac{b_i}{a_i + b_i} \tag{18}$$

$$\bar{b_i} \triangleq \frac{a_i}{a_i + b_i} \tag{19}$$

where a_i is the distance from the point measurement to the centre of the i^{th} step, and b_i is the distance from the point measurement to the centre of the $(i+1)^{th}$ step. We then obtain the thickness estimates $\boldsymbol{t}$ by solving the linear least squares in closed form,

$$\hat{\boldsymbol{t}} = \underbrace{(\boldsymbol{W}^t \boldsymbol{W})^{-1} \boldsymbol{W}^t (\boldsymbol{y} - y_0)}_{h^{-1}(\boldsymbol{y})}. \tag{20}$$

Therefore, $\hat{\boldsymbol{t}}$ are calculated as a pseudo inverse from the forward model and can even be done as the robotic tool travels through the pipe. Section 3 presents the evaluations carried out for both forward and inverse models.

3 Results

FEA simulations with a 2D cross-sectional geometry have been used to validate the proposed methods in a controlled environment. The performance of both the forward and inverse model has been analysed by applying them to a realistic known pipe profile.

3.1 FEA environment

This section describes how the data for the formulation was obtained. Realistic real life cross-sectional thickness profiles were used in the FEA environment to collect the data sets. Pipe sections exhumed from a test bed situated in Strathfield, Sydney were used for the forensic analysis of the real thickness profile.

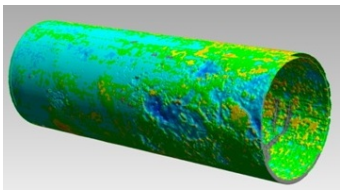

(a) 3-D model

(b) 3-D laser scanner

Figure 5: 3-D model generated from the laser scanner

This particular pipeline was laid more than a century ago with an original manufactured wall thickness of 30mm. However, after the years of service, some parts of the pipe have been significantly corroded. Some pipe sections were exhumed and grid-blasted to remove all non-metallic substances formed on the pipe surface. The corroded cross-sectional thickness profiles have been captured with the 3D laser scanner shown in Figure 5b. The 3D point cloud generated from the scanner was later ray traced as described in [Skinner *et al.*, 2014] to extract the cross-sectional ground-truth.

Each dataset consists of an equivalent 192m long 1-D profile based on the geometry of exhumed pipe segments. Once incorporated into a FEA simulation environment, this realistic profile has provided sufficient data for validation.

The inspection of a pipe has been simulated using a parameter sweep for the position of the MFL tool within the pipe for the 192m length. The axial component of the magnetic flux leakage density has been recorded for each position of the parameter sweep. The 10mm cement lining present in actual pipes were simulated by keeping the sensor lift-off as 10mm above the pipe surface.

3.2 Forward Sensor Model

Forward sensor model is generated using the data generated as described in Section 3.1. The goal is to learn the parameters defined in Equation (9). Three data sets of 192m each have been used in this work.

For each data set, a three-fold cross-validation process was used to learn the parameters. The estimated $\hat{\boldsymbol{y}}$ and the actual sensor measurements $\boldsymbol{y}$ were calculated for each dataset and compared as a percentage error as shown in Figure 6.

As expected, y_0 converged to a positive value, which indicates the direct coupling field from the exciter magnets. $w_{k/2}$ (centre of the RIO) indicated the highest negative value as the leakage flux increases with lower thicknesses. Further coefficients away from the centre of the Hall effect sensor indicated a decreased negative value finally approaching to zero. This indicates that the thickness values directly below the sensor location have

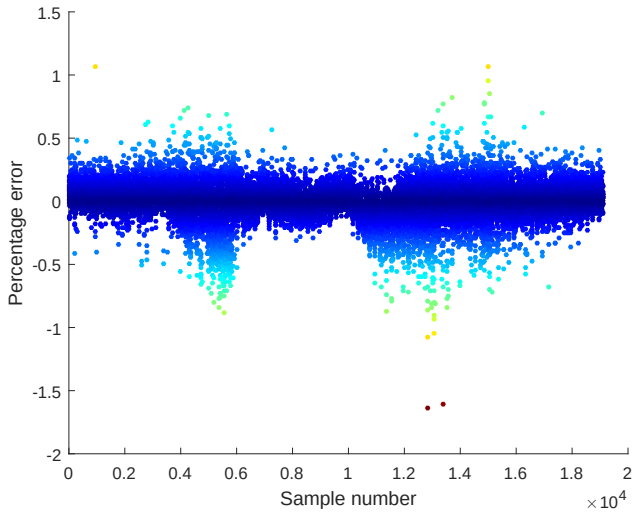

Figure 6: Forward model results data set (a)

Table 2: Forward and inverse model RMS errors

Data set	RMSE	
	Forward Model (T)	Inverse Model (mm)
(a)	8.615×10^{-4}	1.1473
(b)	4.933×10^{-4}	0.6317
(c)	5.9606×10^{-4}	0.3453

a higher impact on the measurement which agrees with the MFL principle.

3.3 Inverse Sensor Model

After optimising the parameters for the forward model, all the parameters required for the inverse model can be calculated. With the three-fold cross-validation, 1/3 of the 192m thickness profile is recovered each time using the formulation established in Section 2.4.

As indicated in the equations in Section 2.4, the solution relies on the parameters learned for the forward problem. In this case, all the parameters about the MFL sensor set-up and the pipe are known, which enables to generate the data using the FEA simulation. Otherwise, multiple calibration data have to be collected experimentally in a known environment. Although practically its an exhausting task, with a reasonable ROI, it is possible to experimentally collect the required data.

A close-up of a section of the recovered pipe profile is indicated in Figure 7. The estimated thickness profile is shown in blue and the ground truth is shown in red.

The inferred thickness profile was directly compared with the ground truth giving a good agreement. RMS error was calculated for each dataset to numerically evaluate the method giving a worst of 1.14mm RMS error for data set (a).

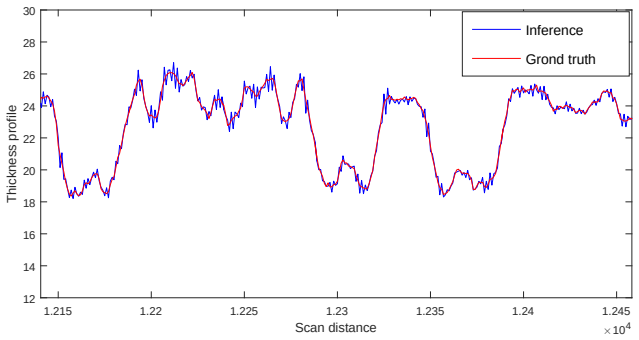

Figure 7: Inverse model results data set (a)

4 Discussion

In this paper, the forward and inverse problems for a MFL sensor have been formulated as linear least squares optimisation problems. The FEA model has been developed using real-life pipe thickness profiles and geometrical values. The forward model was generated based on the FEA data and the closed-form inverse model was formulated using the learnt parameters. As indicated in Section 3, both forward and inverse models provided reasonable estimations of the measurements and thicknesses respectively. Although the results are based on simulations, this approach can be easily extended to work with data from a real tool.

There can be several error sources present in the system. This includes sensor noise, which is assumed Gaussian distributed. It was incorporated in the model by adding noise to FEA simulations. In practice, GMR sensors can minimize such noise effects.

More importantly, the deterministic noise defined by the difference between the linear nature of the proposed model and the real behaviour of the magnetic field is significant. Hence, each MFL point measurement is approximated to a linear combination of the thickness values under the MFL set-up. This generates a simplistic forward model, which allows solving the inverse model with a closed form solution. It is obviously an approximation of the reality for both the direct and inverse models. However, as shown in Figure 6 and Figure 7 it is shown to be an acceptable approximation.

It is to be noted that inhomogeneous magnetic properties of the medium and external sources of electromagnetic fields (i.e. electric power lines or large ferromagnetic objects located near the pipe) can lead to an inevitable error of sensor interpretation. Furthermore, these properties can be affected by the excitation intensity of the exciter coils. The excitation needs to be able to substantially saturate the pipe wall to avoid some of these effects.

In practice, as the in line tool navigates in the pipe, it

is non-trivial to keep a constant lift-off. Since the lift-off has a direct impact on the MFL sensor reading, it should be incorporated into the model. In future, authors are planning to extend this work by incorporating the lift-off values into the model which can be experimentally measured in a practical robotic tool using an inductive or a capacitive type proximity sensors as it travels through the pipe.

References

[Carvalho *et al.*, 2006] A.a. Carvalho, J.M.a. Rebello, L.V.S. Sagrilo, C.S. Camerini, and I.V.J. Miranda. MFL signals and artificial neural networks applied to detection and classification of pipe weld defects. *NDT & E International*, 39(8):661–667, December 2006.

[Edwards and Palmer, 1986] C Edwards and S B Palmer. The magnetic leakage field of surface-breaking cracks. *Journal of Physics D: Applied Physics*, 19(4):657, 1986.

[Falque *et al.*, 2016] R. Falque, T. Vidal-Calleja, G. Dissanayake, and J. Valls Miro. From the Skin-Depth Equation to the Inverse RFEC Sensor Model. *ArXiv e-prints*, September 2016.

[Förster, 1986] F. Förster. New findings in the field of non-destructive magnetic leakage field inspection. *NDT International*, 19(1):3–14, February 1986.

[Ireland and Torres, 2006] R.C. Ireland and C.R. Torres. Finite element modelling of a circumferential magnetiser. *Sensors and Actuators A: Physical*, 129(1-2):197–202, May 2006.

[Khodayari Rostamabad *et al.*, 2009] a. Khodayari Rostamabad, J.P. Reilly, N.K. Nikolova, J.R. Hare, and S. Pasha. Machine Learning Techniques for the Analysis of Magnetic Flux Leakage Images in Pipeline Inspection. *IEEE Transactions on Magnetics*, 45(8):3073–3084, August 2009.

[Mandache and Clapham, 2003] Catalin Mandache and Lynann Clapham. A model for magnetic flux leakage signal. *Journal of Physics D: Applied Physics*, 36:2427–2431, 2003.

[Minkov *et al.*, 2002] D. Minkov, Y. Takeda, T. Shoji, and J. Lee. Estimating the sizes of surface cracks based on Hall element measurements of the leakage magnetic field and a dipole model of a crack. *Applied Physics A: Materials Science & Processing*, 74(2):169–176, February 2002.

[Priewald *et al.*, 2013] R. H. Priewald, C. Magele, P. D. Ledger, N. R. Pearson, and J. S. D. Mason. Fast magnetic flux leakage signal inversion for the reconstruction of arbitrary defect profiles in steel using finite elements. *IEEE Transactions on Magnetics*, 49(1):506–516, Jan 2013.

[Rathnayaka *et al.*, 2016] Suranji Rathnayaka, Robert Keller, Jayantha Kodikara, and Li Chik. Numerical simulation of pressure transients in water supply networks as applicable to critical water pipe asset management. *Journal of Water Resources Planning and Management*, 142(6):04016006, 2016.

[Skinner *et al.*, 2014] Bradley Skinner, Jaime Vidal-Calleja, Teresa amd Valls Miro, Freek De Bruijn, and Raphael Falque. 3D point cloud upsampling for accurate reconstruction of dense 2.5D thickness maps. In *Proceedings of the Australasian Conference on Robotics and Automation 2014 (ACRA 2014)*, pages 1–7, Melbourne, Australia, 2014. Australian Robotics and Automation Association Inc.

[Uetake and Saito,] I. Uetake and T Saito. Magnetic flux leakage by adjacent parallel surface slots. *NDT & E International*.

[Wijerathna *et al.*, 2013] Buddhi Wijerathna, Teresa Vidal-Calleja, Sarath Kodagoda, Qiang Zhang, and Jaime Valls Miro. Multiple defect interpretation based on gaussian processes for mfl technology. In *SPIE Smart Structures and Materials+ Nondestructive Evaluation and Health Monitoring*, pages 86941Z–86941Z. International Society for Optics and Photonics, 2013.

[Wijerathna *et al.*, 2015] B. Wijerathna, S. Kodagoda, J. V. Miro, and G. Dissanayake. Iterative coarse to fine approach for interpretation of defect profiles using mfl measurements. In *Industrial Electronics and Applications (ICIEA), 2015 IEEE 10th Conference on*, pages 1099–1104, June 2015.